Preprint of: Pierpaoli M., Jakóbczyk P., Szopińska M., Ryl J., Giosué Ch., Wróbel M., Strugala G., Łuczkiewicz A., Fudala-Książek S., Bogdanowicz R. (2025). Optimizing electrochemical removal of perfluorooctanoic acid in landfill leachate using ceramic carbon foam electrodes by coupling CFD simulation and reactor design. Chemosphere, 376, 144282. https://doi.org/10.1016/j.chemosphere.2025.144282

Submitted version – Online: 10.1016/j.chemosphere.2025.144282

Optimizing electrochemical degradation of perfluorooctanoic acid in landfill leachate using ceramic carbon foam electrodes by coupling CFD simulation and reactor design

Mattia Pierpaoli[a], Pawel Jakobczyk[a], Małgorzata Szopińska[b], Jacek Ryl[c], Chiara Giosué[d], Maciej Wróbel[a], Gabriel Strugala[e], Aneta Luczkiewicz[b], Sylwia Fudala-Ksiazek[f], Robert Bogdanowicz[a]

[a] Faculty of Electronics, Telecommunications and Informatics, Department of Metrology and Optoelectronics, Gdańsk University of Technology, 11/12 Gabriela Narutowicza Street, 80-233 Gdańsk, Poland; mattia.pierpaoli@pg.edu.pl (MP, *Corresponding Author*, Tel +48 58 3471503 Fax +48 58 3471848) pawel.jakobczyk@pg.edu.pl (PJ) maciej.wrobel@pg.edu.pl (MW) robbogda@pg.edu.pl (RB)

[b] Faculty of Civil and Environmental Engineering, Department of Environmental Engineering Technology Gdańsk University of Technology, 11/12 Gabriela Narutowicza Street, 80-233 Gdańsk, Poland; malszopi@pg.edu.pl (MS) ansob@pg.edu.pl (AL)

[c] Faculty of Applied Physics and Mathematics, Division of Electrochemistry and Surface Physical Chemistry, Gdańsk University of Technology, 11/12 Gabriela Narutowicza Street, 80-233 Gdańsk, Poland; jacryl@pg.edu.pl (JR)

[d] Department of Materials, Environmental Sciences and Urban Planning (SIMAU), Università Politecnica delle Marche, Via Brecce Bianche 12, 60131 Ancona, Italy; c.giosue@univpm.it (CG)

[e] Department of Materials Science and Technology, Institute of Manufacturing and Materials Technology, Faculty of Mechanical Engineering and Ship Technology, Gdańsk University of Technology, 11/12 Gabriela Narutowicza Street, 80-233 Gdańsk, Poland; gabriel.strugala@pg.edu.pl (GS)

[f] Faculty of Civil and Environmental Engineering, Department of Sanitary Engineering, Gdańsk University of Technology, 11/12 Gabriela Narutowicza Street, 80-233 Gdańsk, Poland. sksiazek@pg.edu.pl (SFK)

Abstract

Perfluorooctanoic acid (PFOA), a persistent and bioaccumulative pollutant classified as a 'forever chemical', poses a global environmental and health risk due to its widespread use and resistance to degradation. The development of effective and efficient removal technologies is crucial to mitigate its long-term impacts. In this study, we present a novel approach to address the growing concern of emerging contaminants, particularly PFOA, in landfill leachate. We investigate the use of ceramic carbon foam electrodes (CCFE) as a cost-effective and efficient alternative to traditional electrode materials for the electrochemical degradation of PFOA. Micro-computed tomography was used to reconstruct the actual three-dimensional geometries of the samples in which porosities were calculated. We also coupled computational fluid dynamics simulations of the actual geometries and optimised the working conditions to

minimise pressure drop and improve treatment efficiency. Our design significantly reduces energy requirements by operating at lower potentials, a critical factor in sustainable waste management practices. The optimised CCFE system demonstrated superior performance in the degradation of PFOA in landfill leachate, offering a promising solution for the treatment of emerging contaminants. This study not only provides a viable method for mitigating the environmental impact of PFOA, but also sets a precedent for the development of low-energy, high-efficiency treatment technologies for various persistent pollutants. In addition, the proposed solution, as part of closed-loop water systems, will enhance water reuse and recycling, thereby preserving and regenerating natural water bodies.

Keywords

PFAS, electrochemical oxidation, advanced oxidation process, electrode stability

1. Introduction

The global increase in the volume and complexity of waste poses serious risks to ecosystems and human health (Clift et al., 2018; Falandysz et al., 2022). These growing waste streams are a combined source of emerging contaminants, including per- and polyfluoroalkyl substances (PFAS) (Reinhart et al., 2023). Due to the strong carbon-fluorine (C-F) bond, the persistent nature of PFAS allows them to persist in the environment, accumulate in soil and water, and thereby enter the food chain (Wee and Aris, 2023; Zafeiraki et al., 2019), raising significant health concerns. These concerns include the potential for both chronic and acute adverse human health effects, such as developmental problems, liver damage and an increased likelihood of cancer (Goodrich et al., 2022), as well as effects on wildlife (De Silva et al., 2021; Zafeiraki et al., 2019). Although many environmental contaminants are regulated and managed, effective control measures for PFAS and similar emerging contaminants remain inadequate. In particular, there is an urgent need for cost-effective technologies to remove persistent contaminants before they are released to the environment (Brunn et al., 2023;

Falandysz et al., 2022), especially from landfill leachates (Pierpaoli et al., 2021b). Efforts to remove PFAS from water include activated carbon adsorption and various physical and chemical treatments such as reverse osmosis, nanofiltration, ultrafiltration, oxidation and ion exchange, as well as biological treatments including biodegradation and constructed wetlands (EUN et al., 2022; Lu et al., 2023). Despite their effectiveness, these treatments are costly and result in PFAS-containing waste, which poses disposal challenges. Innovative technologies, such as electrochemical methods, offer promising alternatives for the treatment of PFAS-contaminated waters (Pierpaoli et al., 2021b; Xiao et al., 2023). These methods are valued for their versatility and cost-effectiveness, using electrons to directly or indirectly oxidise contaminants. A major focus is the use of three-dimensional electrodes, which come in various forms such as meshes, foams and porous solids, and are effective in increasing the rate of redox reactions. The movement of mass towards the electrode surfaces involves migration, convection and diffusion. The role of mixing in this context is twofold. Firstly, it helps to uniformise the concentration of reactants within the solution, ensuring a consistent and homogeneous mixture; secondly, it helps to reduce the thickness of the Prandtl layer immediately adjacent to the electrode surface.

The adsorption and electrochemical oxidation (EO) of perfluorooctanoic acid (PFOA) using unconventional materials have received considerable attention due to their low cost, high efficiency and environmental friendliness. While no adsorption of PFOA was observed on the negatively charged silica surface, PFOA and other PFASs were found to sorb to the alumina surface (positively charged), forming a hydrated layer, suggesting that the adsorption process appears to be driven by electrostatic interactions between the PFAS functional group (negative) and the mineral surface (Hellsing et al., 2016). Hydrotalcite is a layered double hydroxide (LDH) with the general formula $Mg_6Al_2CO_3(OH)_{16}$-$4H_2O$ and has been shown to have extraordinary adsorption capacities for PFOA, of the same order as anionic exchange resins (above 100 mg/g) (Alonso-de-Linaje et al., 2021). Similarly, Wang and Shish showed how PFOA adsorption on crystalline alumina is influenced by the pH of the solution and how it decreases with increasing ionic strength of the cations, due to the compression of the electrical

double layer, as both Ca and Mg can form bridges with PFOA anions in solution (Wang and Shih, 2011). In fact, PFOA adsorption on inorganic oxide materials is mostly driven by electrostatic interactions (Chen et al., 2021). Al oxides and hydroxides, such as those derived from aluminium-based drinking water treatment residuals, have also been shown to strongly adsorb PFOA, with the capacity decreasing with increasing pH (Zhang et al., 2021). Open-cell foams have attracted considerable attention for various applications, such as catalytic substrates in combustion, reformers and converters to control pollutant emissions. They have also been of interest in the energy sector, particularly for heat transfer applications and as catalytic substrates in combustion devices, fuel reforming systems and emission control. The appeal of open-cell foams lies in their light weight, high surface to volume ratio and excellent fluid permeability, making them suitable for a wide range of engineering applications. The microstructural geometry of open-cell foams induces a tortuous flow path, resulting in high activity per unit volume, which is particularly advantageous for the aforementioned applications. Researchers have used CFD simulations to study flow regimes within ideal foam structures and the transition from laminar to fully turbulent regimes. Indeed, understanding the pressure drop and flow type as a function of flow rate within such a porous structure is crucial. The Reynolds number has been used to define the flow regime, with smaller pore sizes resulting in lower Reynolds numbers, leading to laminar flow.

The aim of our study was to explore the use of ceramic carbon foam electrodes (CCFE) as a cost-effective replacement for traditional electrode materials in the electrochemical degradation of PFOA found in landfill leachate. We focused on selecting a more affordable material and free from critical raw materials (CRMs) compared to traditionally available options such as boron-doped and metal oxide-coated titanium electrodes (Pierpaoli et al., 2020). Additionally, we optimized the flow and operational conditions using computational fluid dynamics (CFD) simulations, with a particular emphasis on minimizing energy consumption.

2. Materials and methods

2.1 Chemicals and Materials

Perfluorooctanoic acid (PFOA) standard, an analytical standard grade, was purchased from DR Ehrenstorfer (Germany). Eluent additive to HPLC method: ammonium acetate was suitable for mass spectrometry (LiChropur™, Merck Company), while methanol (MeOH), was hypergrade for LC-MS (LiChrosolv®, Merck Company). Phosphate buffer solution (PBS, 0.1 M) was prepared as described in our previous work (Pierpaoli et al., 2021b). Purified water (ultrapure water, resistivity 18.2 MΩ cm at 25°C) was obtained via a Direct-Q® Water Purification System, and used to dilute 1:1 the landfill leachate and spike at different concentrations (0.001, 0.1 and 10 mg L^{-1}) with PFOA. Ceramic carbon foam electrodes (CCFE) were supplied by Ferro-Term (Poland). Briefly, CCFE were prepared from a mixture of ceramic powder, hard coal and carbon binder, suspended in an aqueous silicic acid sol solution. The solution is then used to coat polymer foams, which, after drying, are fired at a temperature of 600-1000°C in an oxygen-free atmosphere.

2.2 CCFE Chemical and morphological characterization

Scanning electron microscopy (SEM) and energy dispersive X-ray (EDX) spectroscopy were performed using a Phenom XL microscope (Thermo Fisher Scientific) with a beam acceleration voltage of 10 kV, operating in high vacuum mode and with a secondary electron detector (SED). Raman spectroscopy was used to study the molecular composition of CCFE. The system consists of a TE-cooled to -60° CCD camera detector (Andor iDus-420-BR-DD, Ireland), a f/2.2 spectrograph with volume phase holographic (VPH) transmission grating (HT-spectrometer, EmVision llc., USA) with dedicated fibre-optic contact probe (EmVision llc., USA) and an excitation laser module with central wavelength of 830 nm (Innovative Photonic Solutions, USA). Micro-computed tomography (µCT) was used for 3D reconstruction of the actual geometry of the samples. The equipment used was a GE phoenix v|tome|xs with an X-ray power set at 30 W (100 kV, 300 µA) and an exposure time of 5000 ms for each radiogram. Additional information on µCT are reported in the supplementary materials. Two copper filters, each with a thickness of 0.5 mm, were used. ICP-OES (Inductively Coupled Plasma -

Optical Emission Spectrometer, Optima 8300 PerkinElmer) analyses were performed on the PFOA solutions, on the LL solution (after 30 minutes the CCFE electrode was in contact with the spiked LL and after full EO test). A constant voltage was then applied and the test was run for 3 hours. The samples collected were 10 mL of liquid for each analytical step. Prior to analysis, the samples were filtered at 45 µm and 0.1 ml of concentrated HNO_3 (ACS acid grade at 65%) was added to prevent precipitation of metals. Each CCFE was used once.

2.3 CCFE Electrochemical characterization

Electrochemical measurements, including Tafel plots, electrochemical impedance spectroscopy (EIS), and potential versus current, were performed before and after electrolysis in a three-electrode system in a beaker with a working electrode (CCFE) measuring 7.5 x 7.6 x 2.5 cm, while the counter (cathode) and reference electrodes were a steel grid and Ad/AgCl wire, respectively. Tafel measurements were recorded from 0 to 4 V at a scan rate of 10 mV/min. A current-potential curve for the CCFE in LL was obtained in the range of -1.5 V to 4 V at a scan rate 20 mV/s. EIS was performed in the frequency range from 1 MHz to 100 mHz, at open circuit potential and with an amplitude of 20 mV. Electrochemical measurements were carried out with a potentiostat-galvanostat (VMP-300, Bio-Logic, France) controlled by EC-Lab software. The electrolyte used for electrochemical measurements was 0.1 M PBS.

2.4 Reactor and monitoring system design

The electrochemical reactor and monitoring cell were designed and realized by additive manufacturing in PETG. Monitoring cell geometry was optimized by CFD simulation, as well as the residence time was estimated to minimize the time between two subsequent samples. The monitoring cell includes 4 low-cost Electrical Conductivity, dissolved O_2 (DO), redox potential, pH sensors (Table S1), which have been calibrated against a laboratory grade digital multimeter (HQ40D, Hach), equipped with HQ2200 (pH); IntelliCAL LDO101 (DO); PT1000 (conductivity) and IntelliCAL MTC101 (redox) probes manufactured by Hach (Germany). The optical cell (Fig. 1B) includes a small cell (10 mm x 10 mm and 6 mm of optical path length) comprised of two quartz glasses. From one of the two sides, the water sample was illuminated

with a halogen source through an optical fibre and a collimator, and the resulting spectra were passed through collimator and an optical fibre and acquired using a portable UV-VIS spectrometer (Ocean Optics FX). For the monitoring and optical cells, two peristaltic pumps regulated the flow. All optical and chemical measurements were conducted under static conditions, meaning there was no flow during these measurements. Leachate was directed to the measurement cells at five-minute intervals for sensor analysis. Additionally, samples taken at specific time intervals - 0, 5, 15, 30, 60, 90, 120, and 150 minutes - were specifically designated for analysis using ultra-high performance liquid chromatography tandem mass spectrometry with electrospray ionisation (UHPLC-ESI-MS/MS). The electrochemical reactor was designed as a parallelepiped chamber to facilitate flow through the CCFE electrode, with the inlet and outlet positioned at diametrically opposed openings in the reactor (Fig. 1C). For each experiment, the system was allowed to stabilise for 30 min before a constant voltage was applied. This stabilisation period ensured that the adsorption on the electrode reached a steady state. A constant potential was then maintained for 180 minutes in each experiment, with the current measured continuously throughout the process.

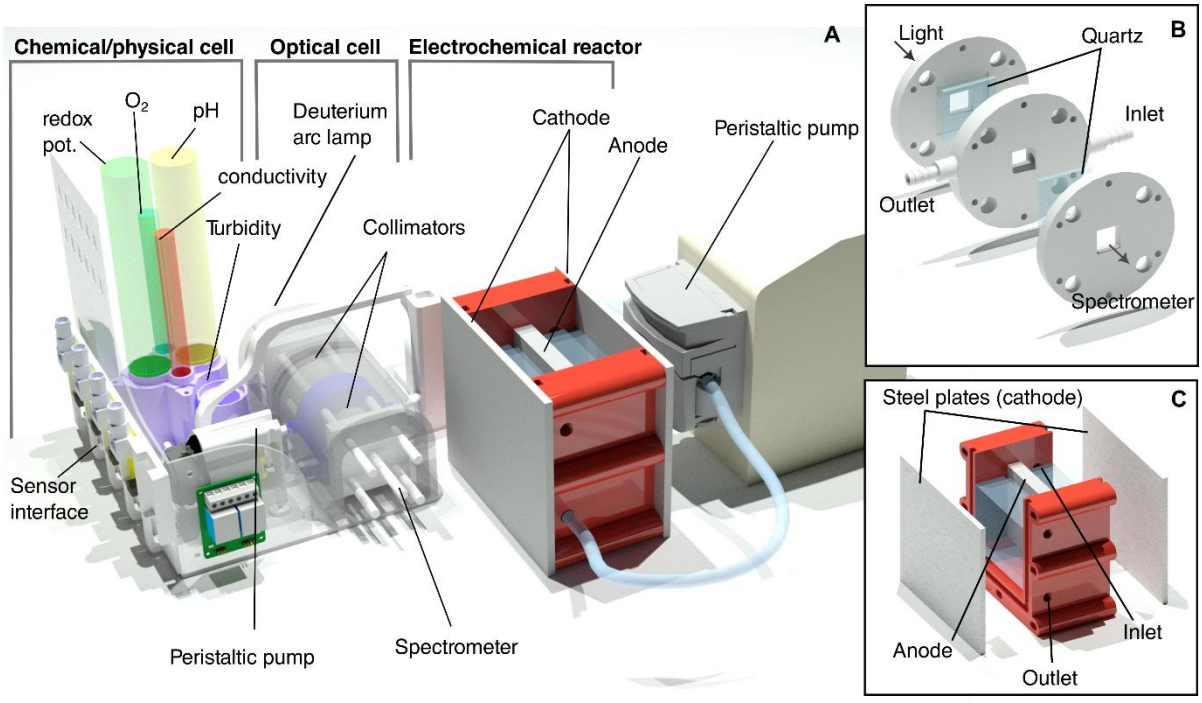

Fig. 1. – (A) Setup for the EO tests; (B) Optical cell;(C) EO reactor

The energy consumption per unit mass of PFOA removed (EC_{PFOA}) for the electrochemical mineralization process at a giving reaction time t (h) was calculated as [29]:

$$EC_{PFOA} = \frac{E_{cell} I t}{\Delta[PFOA]_t V} \qquad \text{Eq. 1}$$

where E_{cell} is the cell potential (V), I the applied electric current (A), $\Delta[PFOA]_t$ (mg L^{-1}) the variation of [PFOA] after a certain time t (h), and V the solution volume (L).

2.5 Adsorption experiments

Adsorption isotherm experiments were carried out in 120 mL HDPE vessels containing 100 mL solution. The initial concentrations of PFOS varied from 0.02 mg L^{-1} to 0.5 mg L^{-1} and from 10 mg L^{-1} to 125 mg^{-1} to achieve two adsorption isotherms at low and high concentrations. The vessels were shaken for 24 h. The amount of PFOS adsorbed by the CCFE and the single-point adsorption coefficients K_d (L g^{-1}) were calculated from

$$q_t = \frac{C_0 - C_t}{C_s} \qquad \text{Eq. 2}$$

$$K_d = \frac{q_e}{C_e} \qquad \text{Eq. 3}$$

where q_t and q_e (μmol g^{-1}) are the concentrations of solutes adsorbed on the adsorbents at time t (min) and at equilibrium, respectively. C_o (μmol L^{-1}) is the initial solute concentration. C_t and C_e (μmol L^{-1}) are the solute concentrations in the aqueous phase at time t and at equilibrium, respectively. C_s (g L^{-1}) is the mass of the CCFE.

The solid–liquid sorption distribution coefficient, K_d (mL g^{-1}), was calculated as the ratio between the PFOA concentration sorbed in CCFE, C_s (mg g^{-1}), and its concentration in the aqueous phase at equilibrium, C_{eq} (mg L^{-1}):

$$K_d = \frac{C_s}{C_{eq}} \qquad \text{Eq. 4}$$

C_{eq} values were directly determined by UPLC–MS/MS and the corresponding concentrations of PFASs sorbed by CCFE, whereas Cs was calculated by the following equation:

$$C_s = \frac{(C_{in} - C_{eq})V}{m_{CFFE}} \qquad \text{Eq. 5}$$

where C_{in} (mg L^{-1}) corresponds to the initial concentration of PFOA added to the CCFE, V (mL) is the volume of solution and m_{CCFE} (g) refers to the dry mass of the CCFE.

The Freundlich model is quantitatively described by the following equation:

$$C_s = K_f C_{eq}^n \qquad \text{Eq. 6}$$

Where K_f is the Freundlich constant, related to the adsorption capacity of the adsorbent and the intensity of adsorption and n is the Freundlich exponent, a dimensionless constant that represents the heterogeneity of the adsorption sites on the solid surface. The K_f and n parameters of the Freundlich equation were calculated by non-linear least squares fitting of the sorption isotherms.

2.6 UHPLC – MS/MS and chemical analysis

An UHPLC-ESI-MS/MS Nexera XR coupled with LC/MS-8050 (Shimadzu Company), was used to determine PFOA concentration. Process control samples were filtrated via polypropylene (PP) 0.45 µm pore size syringe filters (Whatman®) and directed to UHPLC-ESI-MS/MS analysis. Modified and adjusted to the study purposes EPA 537.1 method was applied. Shim-pack SP-C18, 2.1 x 150 mm, and 2.7 µm was used as an analytical column, with a constant flow applied at 0.3 ml min^{-1}. The sample injection volume was 1 or 5 µL (depending on the spiking level). The calibration curve was plotted using 5-level calibration (linearity in the ranges of 1–100 µgL^{-1} and 1-10 mgL^{-1}). The method detection limit (MDL) and method quantification limit (MQL) were 1 and 3 µgL^{-1} for the landfill leachate matrix. For this method, no analyte pre-concentration was applied. Additional details are reported in the supplementary materials. The composition of the landfill leachate was analysed using the methods described in detail in our previous work (Fudala-Ksiazek et al., 2018; Szopińska et al., 2021; Wilk et al., 2022).

2.7 CFD simulation

A aomprehensive review on modelling turbulent flows in porous media, among which metal foams, has been done by Wood, He and Apte (Wood et al., 2020). Briefly, in porous media, four distinct flow regimes can be identified: (a) Darcy, (b) Forchheimer, (c) unsteady laminar

(transitional), and (d) fully-turbulent regime (Dybbs and Edwards, 1984). The transition between these regimes is described by the pore-based Reynolds number, given by the formula:

$$Re_p = \frac{UL_p}{\nu} \qquad \text{Eq. 7}$$

In which L_p is assumed equal to the diameter of the average pore size, U is the intrinsic average velocity and ν the kinematic viscosity.

Firstly, by considering a 20 x 20 x 60 mm representative elementary volume (REV), steady Reynolds-averaged Navier–Stokes (RANS) simulations were performed at various Re number. The REV was obtained by μCT of the real sample and subsequent the mesh was reconstructed by voxel segmentation. Meshing (4.5×10^6 elements) and CFD simulations were performed with COMSOL Multiphysics 6.1.

The v^2-f model (Durbin, 1991), a higher order turbulence model, suggested to be particularly suitable for turbulent flow in coarse porous media (Kazerooni and Hannani, 2007), has been chosen. Then CFD simulation at different flow rates have been performed, in order to obtain the averaged values for permeability to describe the macroscopic model. Permeability, κ, is given by the Eq. 8

$$\kappa = u_{out}\mu\frac{L}{\Delta p} \qquad \text{Eq. 8}$$

Where μ is the dynamic viscosity, u_{out} the outlet fluid velocity in the flow direction, L the side length and Δp the pressure drop across the REV. κ has been calculated for low velocities (equivalent to $Re_p < 12$), for which we found a linear relation was still valid.

Secondly, the reactor reported in Fig. 1c has been simulated, using a porous media characterized by porosity ε_p and permeability κ as the CCFE with the additional Forchheimer coefficient equal to:

$$\beta = \frac{\rho\varepsilon_p C_f}{\sqrt{\kappa}} \qquad \text{Eq. 9}$$

Having ρ the fluid's density and C_f the dimensionless Friction coefficient (Amiri and Vafai, 1998), equal to 0.23 (Amiri and Vafai, 1998).

3. Results and discussion

3.1. Landfill leachate characterization

The landfill leachate (LL) was taken from the municipal solid-waste plant (MSWP) 'Eko Dolina Lezyce' located in the Pomerania region (northern Poland) from the cell operated during a period where there was no waste segregation (from 2003 to 2011). This may cause various micropollutant presence in the samples (including contaminants from the perfluorinated organic compounds). The samples of raw LL were collected to polyethylene bottles in August 2022 and transported to the laboratory (at 4 ± 1°C), where their physicochemical properties were immediately evaluated. The basic composition of the landfill leachate is summarised in Table S2.

3.2. Setup characterization and parameter optimization

CCFE is characterized by a three-dimensional connected mesh structure and high porosity, small flow resistance and it is electrically conductive. The fabrication of CCFE is conducted via a multi-stage procedure. The process starts with the application of a ceramic suspension, comprising alumina, sintering coal, and a blend of additives, onto an elastic polymer foam. This slurry is employed to impregnate the polymeric foam, which acts as a foundational skeleton for the ensuing structure. Following the application of the slurry, the foam filters are subjected to a drying phase. Then, filters are placed in a kiln and exposed to elevated temperatures. During the firing phase, the organic skeleton within the filters is incinerated, resulting in an interconnected, porous ceramic matrix. This structure is then sintered to enhance its mechanical strength and durability. Concurrently, caking coal, is added. The heating process induces the caking coal to initially attain a plastic state, facilitating its adherence to and encapsulation of the ceramic component grains. As the temperature increases, the caking coal undergoes sintering, forming a sturdy ceramic-carbon composite material (Asłanowicz et al., 2019; Karwiński et al., 2013).

The resulting solid matrix is a heterogenous composite rich of Al, C, Si oxides (Fig. 2D,E). Fig. 2A presents the 3D reconstruction of the microtomography of the entire CCFE (REV1) employed in the experiments. For more detailed observations of inner pores, a smaller sample

(REV2) was reconstructed at a higher resolution, as illustrated in Fig. 2B. In addition, the diameters of inner pores and voids were analysed based on microphotographs taken by SEM (Fig. 2C). From SEM/EDX analysis (Fig. 2D) it is possible to see that the composition of the raw CCFE accounts mostly of Al, C, Si and Na (Fig. 2E). The total porosity is a complex outcome influenced by the sacrificial polymeric structure, which is skeletal and characterized by a high void content, along with the presence of inner pores. The volume of inner pores has been calculated for both REV samples, and the distribution is depicted in Fig. 2F. The inner pore diameters, shown in Fig. 2G, were in the range of tens of micrometers, and the distribution of void diameters, as shown in the same figure, had a median diameter of approximately 3.8 mm. Full porosity calculations for both samples based on 3D reconstructions are shown in Table 1. The total porosity of the REV1 sample was 72.4%, while that of the REV2 sample was 79.6%. The differences in porosity between the samples are attributed to the different volumes used for calculations and the different resolutions (voxel size) obtained. In addition, the surface area of the samples that were counted is given in Table S3.

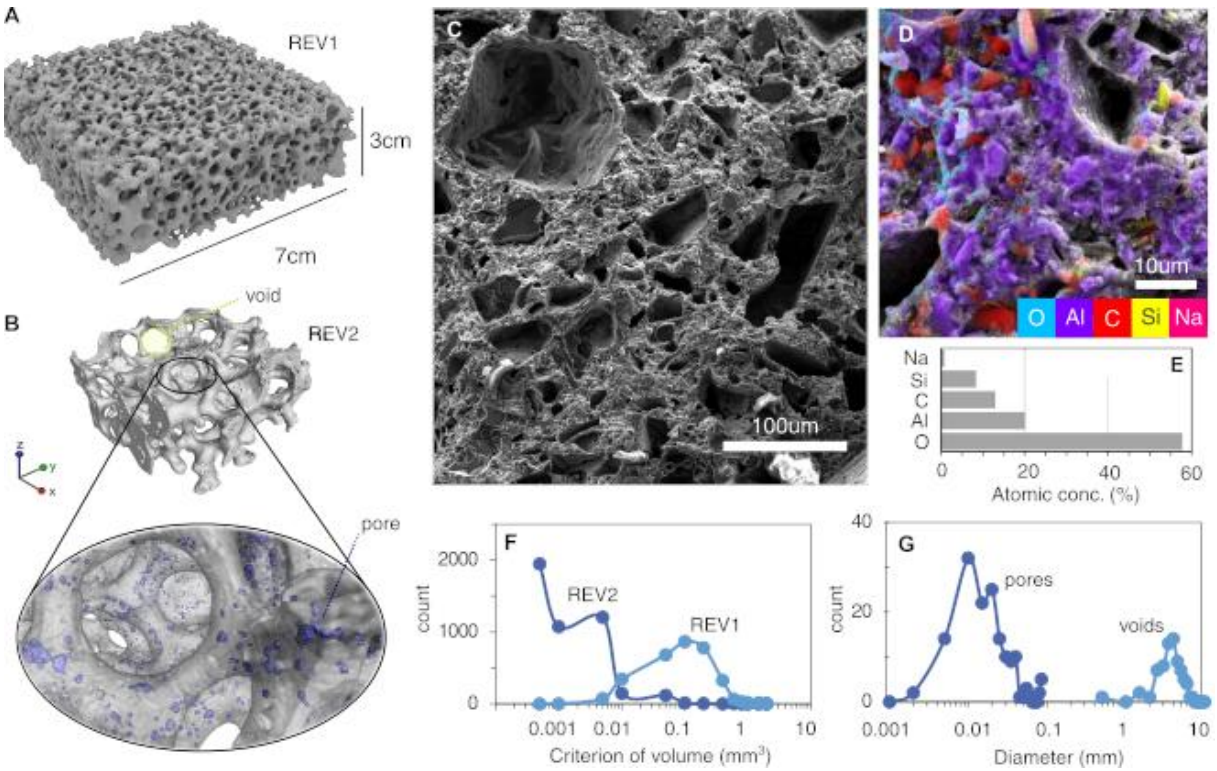

Fig. 2. – A) 3D visualization of a reconstructed larger sample; B) 3D visualization of a reconstructed smaller sample with marked void and a magnified semi-transparent image showing pores; C) Cross-

section of sample observed by SEM; D) Map of elements on the cross-section of the sample observed by SEM and EDX; E) Elemental analysis of the sample; F) Volume distribution of pores and (G) diameter distribution of pores and voids of the REVs.

3.3. PFOA oxidation in landfill leachate

A current-potential curve for the CCFE in LL was obtained by scanning from -1.5 V to 4 V (vs Ag/AgCl 3M KCl). From Fig. 3A it is possible to observe two linear trends from which two potentials, 2.5 V and 4 V, have been selected to perform the EO experiment under potentiostatic conditions.

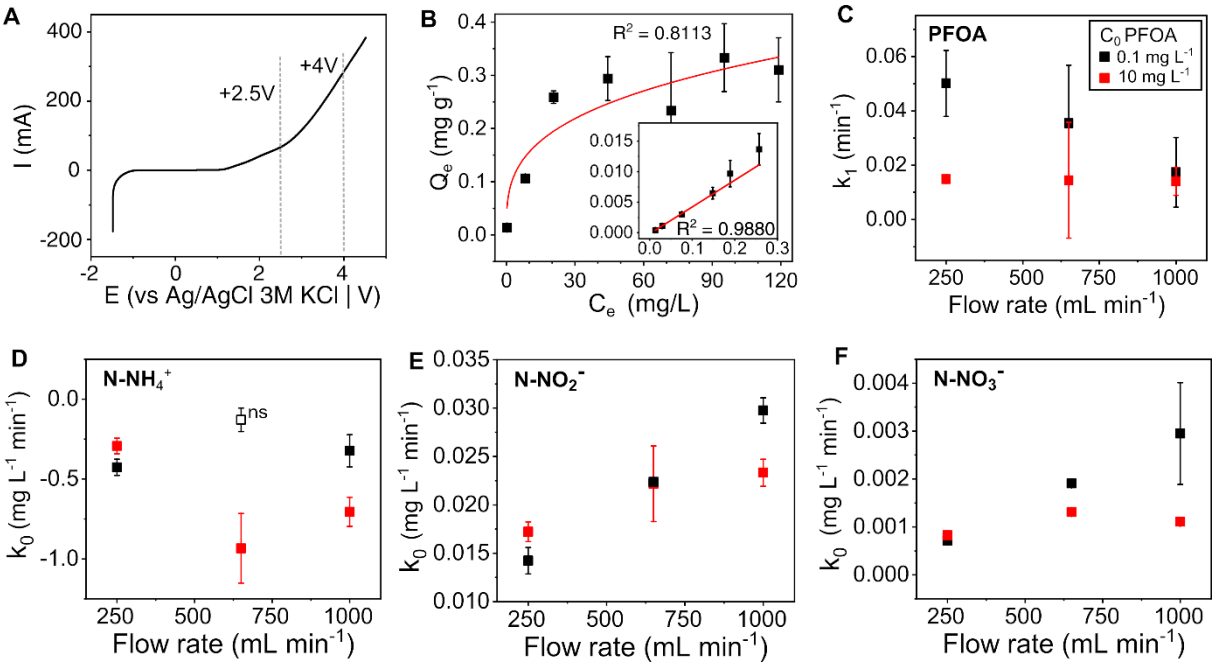

Fig. 3. - A) Potential vs current for CCFE in LL; B) PFOA adsorption isotherms at high and low (inset) concentrations for the CCFE electrode; C) PFOA degradation rate as function of the flow rate. Zero-order rate constants for; D) N-NH_4^+; E) N-NO_2^- and F) N-NO_3^- as function of the flow rate. "ns": not significant for $p > 0.05$.

The adsorption of PFAS on various carbonaceous and inorganic materials has been extensively described and reviewed elsewhere (Du et al., 2014; Valencia et al., 2023). C_s vs. C_{eq} plots were used to construct sorption and then fitted to both Freundlich and linear models, which are commonly used for hydrophobic compounds (Hinz, 2001) and have been previously applied to describe PFAS sorption in sediments (Du et al., 2014; Hellsing et al., 2016; Higgins and Luthy,

2006). For low PFOA concentrations (0.02-0.5 mg L^{-1}), a linear relationship was observed with a K_d of 0.05 mL/mg, while for higher PFOA concentrations (10-125 mg L^{-1}), the Freundlich isotherm fit the experimental results with a K_f of 0.078 $mg^{(1-n)}mL^n$ g^{-1} (Fig. 3B). A comparison with similar adsorbents by composition is given in Table S4. The first order rate constants of PFOA as a function of both initial concentration and flow rate are shown in Fig. 3C. It can be observed that at lower concentrations, the slower the flow through the CCFE, the higher the rate constant. While this may seem counterintuitive, since a higher flow rate implies a higher mixing rate, which has been reported in the literature to enhance PFOA oxidation (Asadi Zeidabadi et al., 2023), it also implies a lower residence time in the reactor and a lower contact time with the CCFE surfaces. Since PFOA oxidation is mostly driven by direct electron transfer, rather than the action of the $^{\bullet}OH$ radical (Pierpaoli et al., 2021b), where the limiting step is provided by the electrode active surface, the higher velocity through the CCFE results in a lower rate. Furthermore, we observed that no degradation occurs at the lower potential of +2.5 V (Fig. S1). A zero-order reaction was observed for ammonium removal, as it may be mainly driven by the indirect pathway through reaction with chlorine (Li and Liu, 2009), which is abundant in LL. Fig. 3D shows the variation of the ammonia rate constant as a function of the flow rate. While the NH_4^+ concentration decreases as the EO process progresses, the $N\text{-}NO_2^-$ and $N\text{-}NO_3^-$ concentrations increase, also clearly at zero order, as ammonia is partially converted to nitrate ions (Anglada et al., 2011; Pierpaoli et al., 2021a). While a correlation between flow rate and $N\text{-}NH4^+$ removal rate is not visible, it is for the $N\text{-}NO_2^-$ and $N\text{-}NO_3^-$ rates, as they increase with increasing flow but they are less affected from the presence of PFOA, due to competitive direct oxidation on the surface electrode. The COD is slightly affected by the EO, since its degradation is accompanied by the release of carbon from the electrode (Fig. S2).

The optical transmittance of the LL was measured using the designed optical cell, with a halogen lamp as the source, in the ranges 350-550 nm and 670-950 nm. The 550-670 nm interval was discarded due to the presence of the lamp emission peak which saturated the spectroscope. When a potential of +4 V was applied, the transmittance in the range 400-550 nm decreased, which may be due to carbon loss from the electrode to the LL. Additionally, a

slight increase in transmittance was observed in the range 670-780 nm when a potential of +2.5 V was applied. An increase was also observed in the blank sample without the application of a potential. This increase is likely due to the sedimentation and/or adsorption of particles and compounds (Fig. S3). Fig. S4 shows the correlation between the parameters estimated by the chemical/physical monitoring cell. A general decrease in LL pH is observed, along with a slight increase in electrical conductivity. The oxidation reduction potential decreases abruptly from positive (84±18)mV to negative (-66±12)mV just 15 minutes after the application of the potential difference, and slowly increases with time to (-43±24)mV at 150 minutes. Oxygen is rapidly depleted as it is consumed in the cathode, reaching its minimum after one hour of treatment. However, a higher flow rate supports the LL reoxygenation (see Fig. S5). The specific energy consumption for PFOA removal, as described in Eq. 1, decreases with increasing PFOA concentration, in a log-log correlation (Fig. S6).

3.4. Uniform corrosion rate and local corrosion susceptibility evaluation

To evaluate the susceptibility of uniform corrosion rate, the electrodes underwent cyclic polarization and electrochemical impedance spectroscopy measurements before and after an electrolysis event. Three external environmental factors were identified as important for material degradation rate and electrolytic efficiency: electrolyser polarization conditions, hydrodynamic fluid flow through the electrochemical cell, and the concentration of contaminant species in the electrolyte. It is important to note that even a single electrolysis cycle can lead to a deterioration in the corrosion resistance of the CCFE electrodes being studied. This can be observed through changes in the electrode's kinetics. Tafel extrapolation can be used to estimate the corrosion current (i_o), which is directly proportional to the corrosion rate. Notably, the electrolysis voltage has a visible effect on the cathodic slope, indicating that both studied polarization conditions: +2.5 and +4.0 V lead to i0 increase by two orders of magnitude, higher at higher polarization voltages (Fig. 4.3A,D). The charge-transfer mechanism shifts from anodically controlled to cathodically controlled after electrolysis.

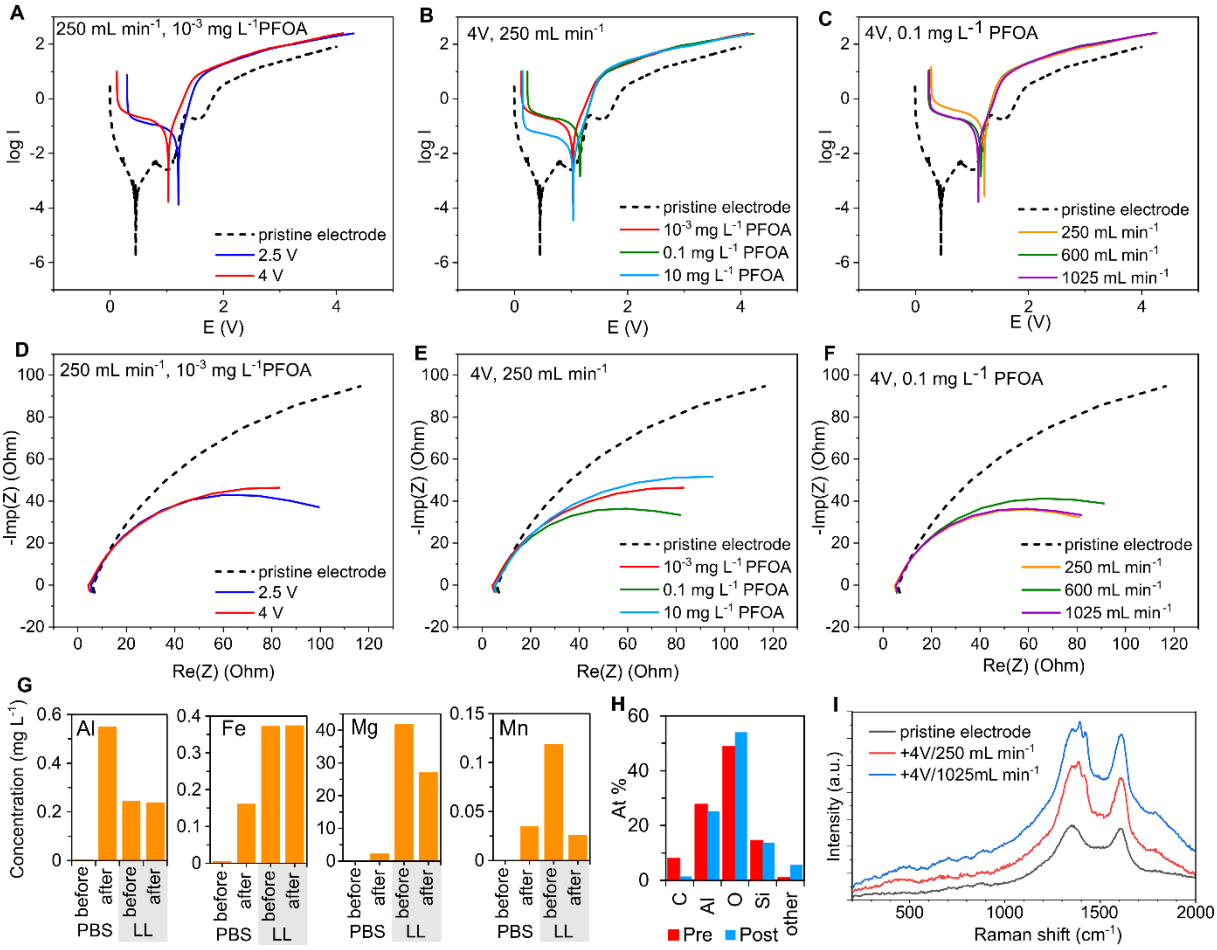

Fig. 4. – (A-C) cyclic polarization curves and (D-F) EIS spectra recorded for CCFE electrodes. (G) Al, Fe, Mg, Mn concentrations, determined by ICP-OES, before and after both pre-conditioning in PBS and in LL. (H) difference in elemental composition, determined by EDX and (I) Raman spectra of the CCFE before and after EO tests.

It is known that some of the electro-oxidized species are adsorbing at the electrode surface, acting as a passive film and effectively blocking the electrode towards consecutive oxidation processes. This characteristic process may lead to a secondary decrease in electrode susceptibility to corrosion, which should be explained by the passivation mechanism. As an example, an effect of Perfluorooctanoic acid (PFOA) was used in different concentrations ranging from 0.001 to 10 mg/L (Fig. 4B,E). Here, at the highest concentrations, the corrosion current i_o was the lowest, which, however, has an expected negative influence on the electro-oxidation efficiency. Notably, there was no shift in the corrosion potential observed, as would be in the case of the classic passive layer. The CCFE corrosion susceptibility was studied at

various hydrodynamic flows, ranging from 250 to 1025 mL/min (Fig. 4.C,F). It is seen that regardless of the flow rate the mechanism of the corrosion process is quite similar, and the corrosion rate is not driven by the diffusion limitation. In other words, despite the flow rate studied the electrochemical process under investigation is activation-controlled, and the electron transfer is slower compared to the diffusion. This observation is connected to the foam shape of the studied electrodes. It should be noted that the lowest i_o was identified for the sample studied at the lowest flow rates.

Part of the Al and Fe content of the CCFE is leached into the PBS prior the electrochemical oxidation test, during the Tafel characterization (Fig. 4G). Moreover, a decrease of Mg and Mn from LL are observed (Chen et al., 2022). The reason may be due the formation of magnesium hydroxide, $Mg(OH)_2$, especially in alkaline conditions, which can precipitate, since it becomes less soluble as the pH increases (Pilarska et al., 2017; Weijma et al., 2022); however, since the pH increases during the process, it may be possible that Mg may be adsorbed/electrodeposited on the electrode or in general, metals can have a rapid aggregation in aqueous solution due to large Van der Waals forces, and decreasing the adsorption potential (Qasem et al., 2021). In fact, according to the reduction at the cathode, the heavy metals solid gathers at the cathode and form a layer on its surface (Tran et al., 2017). Indeed, a reduction was detected on Cr and slightly on Ni (Fig. S7). Additionally, the EDX analysis reveals a loss of carbon content and an enrichment of other elements (Fig. 4H). The Raman spectra collected before and after the EO process show distinct peaks on top of the D peak, broadening of the D peak, and an increase in background fluorescence, possibly due to the loss of carbon from the Al-rich structure (Fig. 4I). The sharper peaks that arise are at approximately 1395 cm^{-1} and 1420 cm^{-1}, which most likely correspond to C—O stretching and CH_2 scissor bending, respectively. Additionally, there is a weak, broad band near the G peak at about 1760-90 cm^{-1}, which is likely attributable to C=O stretching, suggesting oxidation.

In summary, the most notable factor affecting the corrosion rate is the electrode modification under electrolysis, which leads to surface area development and modification of the redox

mechanism. The variation in polarization voltages and flow rates is noticeable but does not exceed one order of magnitude.

3.5. CFD Simulation

The initial step in CFD simulation involved reconstructing the imported REV of the CCFE to eliminate the internal porosity and simplify the geometry through castellation for import into the software. After that, high-order turbulence model (v^2f) has been employed to solve the model. This helps obtain permeability and porosity values, which are then used in an approximate model of the full reactor (Fig. 5A).

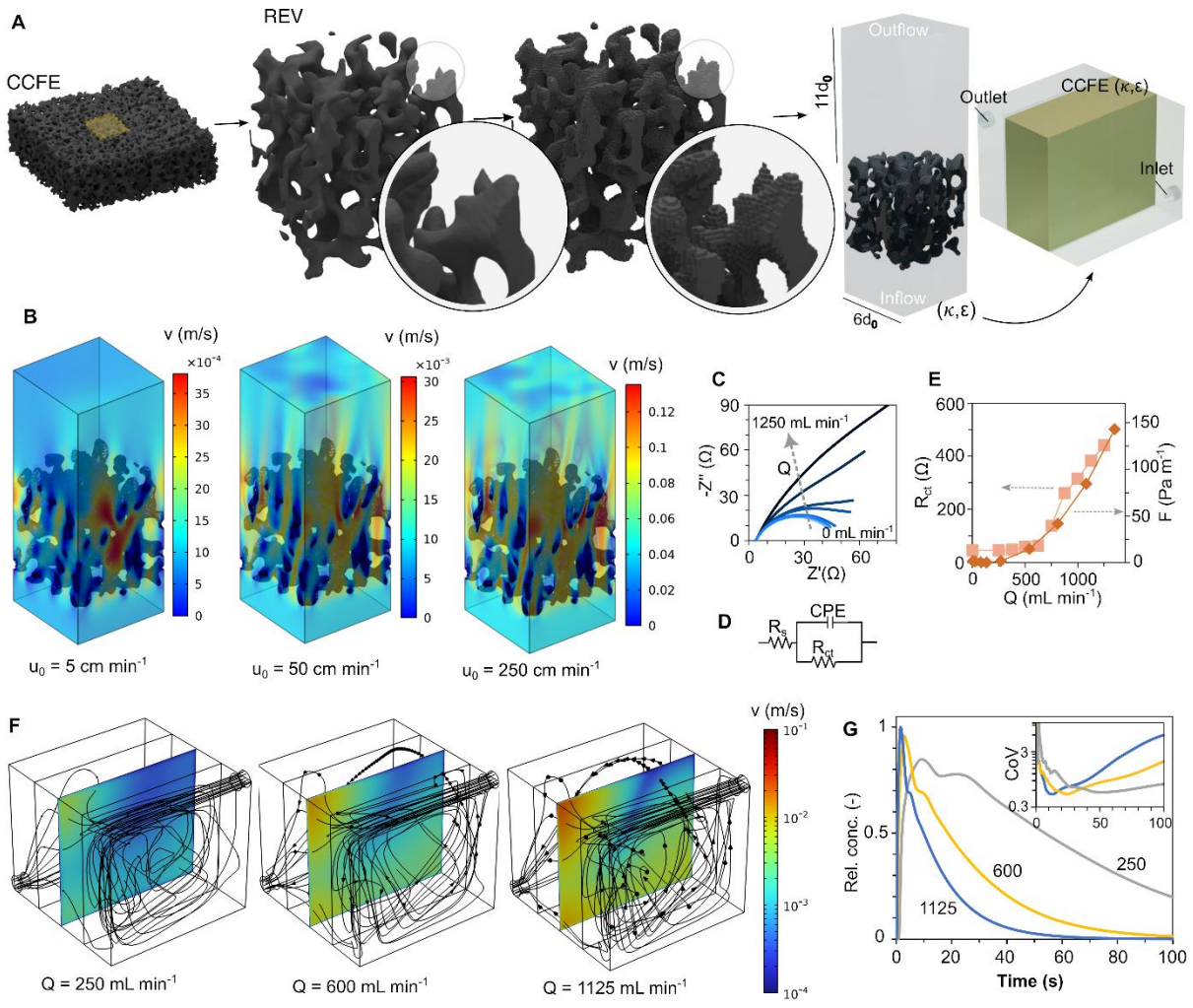

Fig. 5. – (A) schematic representation of the procedure towards the EO reactor CFD simulation. (B) Velocity magnitude across the REV for three selected inlet velocities. (C) EIS results at different flow rates and (D) EEC used to fit the experimental data. (E) Rct and F as function of the flow rate. (F) Velocity magnitudes in the CCFE cross-section at half depth resulting from the simplified CFD

simulation of the EO reactor. (G) Relative concentrations within the CCFE volume as function of the time for an instantaneous release.

Fig. 5B shows the change in the flow field through the CCFE porosity with increasing velocity. The CFD simulation investigated velocities ranging from 1 to 250 cm min^{-1}. Meanwhile, EIS was performed on the CCFE electrode using the setup depicted in Fig. 1. The resulting impedance spectra at various flow rates (ranging from 250 to 1250 mL min^{-1}) are shown in Fig. 5C and fitted with the equivalent electrical circuit (EEC) presented in Fig. 5D. It is noteworthy that R_{ct} increases as the flow rate increases, specifically for Q > 625 mL min^{-1}, which is the threshold at which the Forchheimer contribution (Eq. 9) becomes relevant (Fig. 5D). The increased pressure drop and flow resistance associated with the Forchheimer term (F) affect the transport of species towards the electrode surface, which in turn affects charge transfer kinetics and subsequently the charge transfer resistance of the electrode. The simulation yielded values for porosity and permeability of 0.83 (similar to the total porosity ratio obtained by μCT) and 6.4×10^{-7} m^2, respectively. These values were used to create a simplified model of the reactor. The flow is described by the Navier-Stokes equation in the free region and a Forchheimer-corrected version of the Brinkman equations in the CCFE region. The simulation results at the flow rates used in the EO tests are shown in Fig. 5F. An increasing heterogeneity of velocity intensity can be observed at the centre of the CCFE electrode as the flow rate increases. By simulating an instantaneous release of a given species at the inlet, it is possible to observe concentration peaks at the outlet at 4, 8, and 23 seconds for the three flow rates (Fig. 5G). The latter flow rate has the lowest coefficient of variation (calculated as Fig. S8) and is more constant over time (see inset), suggesting better mixing and concentration uniformity within the CCFE electrode.

4. Conclusions

This study explores the use of CCFE for the electrochemical oxidation of PFOA in landfill leachate. The process parameters, such as applied potential and flow rate, were optimized, and an automated platform was developed to monitor the process, supported by CFD simulations. The PFOA adsorption onto CCFE is comparable to that on Al-rich sediments, and it provides a

valuable support for its electrochemical oxidation. Lower flow-through rates improve PFOA oxidation, while the opposite is true for the oxidation of $N\text{-}NH_4$ to $N\text{-}NO_3$ by $N\text{-}NO_2$. PFOA follows a first-order kinetic due to direct electron transfer being the leading mechanism. In contrast, $N\text{-}NH_4$ oxidation is driven by the indirect reaction with the electrogenerated chlorine, resulting in a zero-order kinetic fashion due to the abundance of chlorides in LL. The results of the CFD simulation indicate that at lower flow rates, the concentration at the CCFE electrode cross-section is more uniform under Darcy flow conditions. Electrode stability was assessed using electrochemical methods, and the leaching of carbon and aluminium was confirmed by EDX and ICP-OES. Additionally, the removal of some metals in the solution, such as Mg and Mn, from LL and their possible deposition onto the electrode surface were detected by means of Raman investigations. By coupling spectroscopic methods with electrochemical ones, it is possible to observe that the transmittance through the LL increases at potentials up to 2.5 V without the oxidation of PFOA. However, at 4 V, PFOA is oxidised, resulting in a decrease in transmittance in the 480-550 nm interval. Additionally, CFD simulations can be used to optimize reactor geometry and operational parameters to develop a viable technology for PFAS control.

Acknowledgements

Funding from the National Science Centre, Poland, under the agreement 2022/45/B/ST8/02847 is acknowledged (M.P.). R.B. acknowledges funding by the National Center for Research and Development through the Project NOR/POLNOR/i-CLARE/0038/2019.

Bibliography

Alonso-de-Linaje, V., Mangayayam, M.C., Tobler, D.J., Rives, V., Espinosa, R., Dalby, K.N., 2021. Enhanced sorption of perfluorooctane sulfonate and perfluorooctanoate by hydrotalcites. Environ. Technol. Innov. 21, 101231. https://doi.org/10.1016/j.eti.2020.101231

Amiri, A., Vafai, K., 1998. Transient analysis of incompressible flow through a packed bed. Int. J. Heat Mass Transf. 41, 4259–4279. https://doi.org/10.1016/S0017-9310(98)00120-3

Anglada, Á., Urtiaga, A., Ortiz, I., Mantzavinos, D., Diamadopoulos, E., 2011. Boron-doped diamond anodic treatment of landfill leachate: evaluation of operating variables and formation of oxidation by-products. Water Res. 45, 828–838.

Asadi Zeidabadi, F., Banayan Esfahani, E., McBeath, S.T., Dubrawski, K.L., Mohseni, M., 2023. Electrochemical degradation of PFOA and its common alternatives: Assessment of key parameters, roles of active species, and transformation pathway. Chemosphere 315, 137743. https://doi.org/10.1016/j.chemosphere.2023.137743

Asłanowicz, M., Ościłowski, A., Lipowska, B., Witek, J., Robak, Z., Muzyka, R., Kowalski, P., Wańczyk, K., 2019. Ceramic-carbon filters for molten metal alloys filtration. Arch. Foundry Eng. 19, 98–102. https://doi.org/10.24425/afe.2019.127101

Brunn, H., Arnold, G., Körner, W., Rippen, G., Steinhäuser, K.G., Valentin, I., 2023. PFAS: forever chemicals—persistent, bioaccumulative and mobile. Reviewing the status and the need for their phase out and remediation of contaminated sites. Environ. Sci. Eur. 35, 1–50. https://doi.org/10.1186/s12302-023-00721-8

Chen, L., Li, F., He, F., Mao, Y., Chen, Z., Wang, Y., Cai, Z., 2022. Membrane distillation combined with electrocoagulation and electrooxidation for the treatment of landfill leachate concentrate. Sep. Purif. Technol. 291, 120936. https://doi.org/10.1016/j.seppur.2022.120936

Chen, Y., Georgi, A., Zhang, W., Kopinke, F.D., Yan, J., Saeidi, N., Li, J., Gu, M., Chen, M., 2021. Mechanistic insights into fast adsorption of perfluoroalkyl substances on carbonate-layered double hydroxides. J. Hazard. Mater. 408, 124815. https://doi.org/10.1016/j.jhazmat.2020.124815

Clift, R., Kaza, S., Yao, L., Bhada-Tata, P., Van Woerden, F., 2018. What a waste 2.0: a global snapshot of solid waste management to 2050, Materials Today. World Bank Publications. https://doi.org/10.1016/S1369-7021(04)00103-8

De Silva, A.O., Armitage, J.M., Bruton, T.A., Dassuncao, C., Heiger-Bernays, W., Hu, X.C., Kärrman, A., Kelly, B., Ng, C., Robuck, A., Sun, M., Webster, T.F., Sunderland, E.M., 2021. PFAS Exposure Pathways for Humans and Wildlife: A Synthesis of Current Knowledge and Key Gaps in Understanding. Environ. Toxicol. Chem. 40, 631–657. https://doi.org/10.1002/etc.4935

Du, Z., Deng, S., Bei, Y., Huang, Q., Wang, B., Huang, J., Yu, G., 2014. Adsorption behavior and mechanism of perfluorinated compounds on various adsorbents-A review. J. Hazard. Mater. 274, 443–454. https://doi.org/10.1016/j.jhazmat.2014.04.038

Durbin, P.A., 1991. Near-wall turbulence closure modeling without "damping functions." Theor. Comput. Fluid Dyn. 3, 1–13. https://doi.org/10.1007/BF00271513

Dybbs, A., Edwards, R. V, 1984. A new look at porous media fluid mechanics—Darcy to turbulent. Fundam. Transp. Phenom. porous media 199–256.

EUN, H., SHIMAMURA, K., ASANO, T., YAMAZAKI, E., TANIYASU, S., YAMASHITA, N., 2022. Removal of perfluoroalkyl substances from water by activated carbons: Adsorption of perfluorooctane sulfonate and perfluorooctanoic acid. Environ. Monit. Contam. Res. 2, 88–93. https://doi.org/10.5985/emcr.20220010

Falandysz, J., Jiménez, B., Taniyasu, S., 2022. Per- and polyfluorinated substances: An environmental update. Chemosphere 291. https://doi.org/10.1016/j.chemosphere.2021.132876

Fudala-Ksiazek, S., Sobaszek, M., Luczkiewicz, A., Pieczynska, A., Ofiarska, A., Fiszka-Borzyszkowska, A., Sawczak, M., Ficek, M., Bogdanowicz, R., Siedlecka, E.M., 2018. Influence of the boron doping level on the electrochemical oxidation of raw landfill leachates: Advanced pre-treatment prior to the biological nitrogen removal. Chem. Eng. J. 334, 1074–1084. https://doi.org/10.1016/j.cej.2017.09.196

Goodrich, J.A., Walker, D., Lin, X., Wang, H., Lim, T., McConnell, R., Conti, D. V., Chatzi, L., Setiawan, V.W., 2022. Exposure to perfluoroalkyl substances and risk of hepatocellular carcinoma in a multiethnic cohort. JHEP Reports 4, 100550. https://doi.org/10.1016/j.jhepr.2022.100550

Hellsing, M.S., Josefsson, S., Hughes, A. V., Ahrens, L., 2016. Sorption of perfluoroalkyl substances to two types of minerals. Chemosphere 159, 385–391. https://doi.org/10.1016/j.chemosphere.2016.06.016

Higgins, C.P., Luthy, R.G., 2006. Sorption of perfluorinated surfactants on sediments. Environ. Sci. Technol. 40, 7251–7256. https://doi.org/10.1021/es061000n

Hinz, C., 2001. Description of sorption data with isotherm equations. Geoderma 99, 225–243.

https://doi.org/10.1016/S0016-7061(00)00071-9

Karwiński, A., Małysza, M., Tchórz, A., Gil, A., Lipowska, B., 2013. Integration of Computer Tomography and Simulation Analysis in Evaluation of Quality of Ceramic-Carbon Bonded Foam Filter. Arch. Foundry Eng. 13, 67–72. https://doi.org/10.2478/afe-2013-0084

Kazerooni, R.B., Hannani, S.K., 2007. Simulation of turbulent flow through porous media employing a v2f model, in: AIP Conference Proceedings. American Institute of Physics, pp. 1257–1260.

Li, L., Liu, Y., 2009. Ammonia removal in electrochemical oxidation: Mechanism and pseudo-kinetics. J. Hazard. Mater. 161, 1010–1016. https://doi.org/10.1016/J.JHAZMAT.2008.04.047

Lu, J., Lu, H., Liang, D., Feng, S., Li, Y., Li, J., 2023. A review of the occurrence, transformation, and removal technologies for the remediation of per-and polyfluoroalkyl substances (PFAS) from landfill leachate. Chemosphere 138824.

Pierpaoli, M., Jakobczyk, P., Sawczak, M., Łuczkiewicz, A., Fudala-Książek, S., Bogdanowicz, R., 2021a. Carbon nanoarchitectures as high-performance electrodes for the electrochemical oxidation of landfill leachate. J. Hazard. Mater. 401, 123407. https://doi.org/10.1016/j.jhazmat.2020.123407

Pierpaoli, M., Rycewicz, M., Łuczkiewicz, A., Fudala-Książek, S., Bogdanowicz, R., Ruello, M.L., 2020. Electrodes criticality: the impact of CRMs in the leachate electrochemical oxidation. Manuf. Rev. 7, 7. https://doi.org/10.1051/mfreview/2020006

Pierpaoli, M., Szopińska, M., Wilk, B.K., Sobaszek, M., Łuczkiewicz, A., Bogdanowicz, R., Fudala-Książek, S., 2021b. Electrochemical oxidation of PFOA and PFOS in landfill leachates at low and highly boron-doped diamond electrodes. J. Hazard. Mater. 403. https://doi.org/10.1016/j.jhazmat.2020.123606

Pilarska, A.A., Klapiszewski, Ł., Jesionowski, T., 2017. Recent development in the synthesis, modification and application of Mg (OH)2 and MgO: A review. Powder Technol. 319, 373–407.

Qasem, N.A.A., Mohammed, R.H., Lawal, D.U., 2021. Removal of heavy metal ions from wastewater: a comprehensive and critical review. npj Clean Water 4. https://doi.org/10.1038/s41545-021-00127-0

Reinhart, D.R., Bolyard, S.C., Chen, J., 2023. Fate of Per- and Polyfluoroalkyl Substances in Postconsumer Products during Waste Management. J. Environ. Eng. 149. https://doi.org/10.1061/joeedu.eeeng-7060

Szopińska, M., Luczkiewicz, A., Jankowska, K., Fudala-Ksiazek, S., Potapowicz, J., Kalinowska, A., Bialik, R.J., Chmiel, S., Polkowska, Ż., 2021. First evaluation of wastewater discharge influence on marine water contamination in the vicinity of Arctowski Station (Maritime Antarctica). Sci. Total Environ. 789, 147912.

Tran, T.-K., Chiu, K.-F., Lin, C.-Y., Leu, H.-J., 2017. Electrochemical treatment of wastewater: Selectivity of the heavy metals removal process. Int. J. Hydrogen Energy 42, 27741–27748.

Valencia, A., Ordonez, D., Sadmani, A.H.M.A., Reinhart, D., Chang, N. Bin, 2023. Comparing the removal and fate of long and short chain per- and polyfluoroalkyl substances (PFAS) during surface water treatment via specialty adsorbents. J. Water Process Eng. 56, 104345. https://doi.org/10.1016/j.jwpe.2023.104345

Wang, F., Shih, K., 2011. Adsorption of perfluorooctanesulfonate (PFOS) and perfluorooctanoate (PFOA) on alumina: Influence of solution pH and cations. Water Res. 45, 2925–2930. https://doi.org/10.1016/j.watres.2011.03.007

Wee, S.Y., Aris, A.Z., 2023. Revisiting the “forever chemicals”, PFOA and PFOS exposure in drinking water. npj Clean Water 6, 1–16. https://doi.org/10.1038/s41545-023-00274-6

Weijma, J., Klok, J.B.M., Dijkman, H., Jansen, G., Sànchez-andrea, I., 2022. Resource Recovery from Water. Resour. Recover. from Water 295–317. https://doi.org/10.2166/9781780409566

Wilk, B.K., Szopińska, M., Sobaszek, M., Pierpaoli, M., Błaszczyk, A., Luczkiewicz, A., Fudala-Ksiazek, S., Krystyna, B., Malgorzata, W., Michał, S., Mattia, S., Agata, P., 2022. Electrochemical oxidation of landfill leachate using boron-doped diamond anodes: pollution degradation rate, energy efficiency and toxicity assessment. Environ. Sci. Pollut. Res. 1–17. https://doi.org/10.1007/s11356-022-19915-3

Wood, B.D., He, X., Apte, S. V., 2020. Modeling Turbulent Flows in Porous Media. Annu. Rev. Fluid

Mech. 52, 171–203. https://doi.org/10.1146/annurev-fluid-010719-060317

Xiao, F., Deng, B., Dionysiou, D., Karanfil, T., O'Shea, K., Roccaro, P., Xiong, Z.J., Zhao, D., 2023. Cross-national challenges and strategies for PFAS regulatory compliance in water infrastructure. Nat. Water 1–12.

Zafeiraki, E., Gebbink, W.A., Hoogenboom, R.L.A.P., Kotterman, M., Kwadijk, C., Dassenakis, E., van Leeuwen, S.P.J., 2019. Occurrence of perfluoroalkyl substances (PFASs) in a large number of wild and farmed aquatic animals collected in the Netherlands. Chemosphere 232, 415–423. https://doi.org/10.1016/j.chemosphere.2019.05.200

Zhang, Z., Sarkar, D., Datta, R., Deng, Y., 2021. Adsorption of perfluorooctanoic acid (PFOA) and perfluorooctanesulfonic acid (PFOS) by aluminum-based drinking water treatment residuals. J. Hazard. Mater. Lett. 2, 100034. https://doi.org/10.1016/j.hazl.2021.100034